Nonthermal solid-solid phase transition in ferromagnetic iron

S. Azadi,[1,*] J.S. Wark,[1] and S.M. Vinko[1,2]

[1] *Department of Physics, Clarendon Laboratory, University of Oxford, Parks Road, Oxford OX1 3PU, United Kingdom*

[2] *Central Laser Facility, STFC Rutherford Appleton Laboratory, Didcot OX11 0QX, UK*

(Dated: December 10, 2024)

We posit the existence of a nonthermal phase transition in iron, driven by a loss of ferromagnetic ordering on ultrafast timescales with increasing electron temperature. The transition corresponds to a solid-solid BCC to FCC phase transformation and takes place at an electron temperature of 0.62 eV while the ion lattice remains near room temperature. The BCC structure initially undergoes phonon softening during the magnetic transformation, followed by a solid-solid phase transition to the FCC structure, and a subsequent hardening of phonon modes. We present a detailed physical picture of the process, supported by finite-temperature density functional theory simulations of the phonon dispersion curves, electronic density of states, and thermodynamic free energy.

I. INTRODUCTION

Short-pulse light sources such as femtosecond optical lasers and x-ray free electron lasers (XFEL) can produce non-thermal and non-equilibrium systems from solids by rapidly driving electrons to high temperatures. Electron excitations generated by ultrafast heating affect the electronic and magnetic structure of the system, its density of states, and lattice vibration spectra, but have also been seen to modify the ionic potential in surprising ways[1–9]. The resulting modified ionic forces can trigger non-equilibrium structural transitions in solids on picosecond timescales, even before any significant energy transfer between electrons and ions can occur[10–13].

To date, the study of non-thermal phase transitions following laser irradiation has predominantly focused on semiconductors. Ultrafast melting under laser excitation was observed by time-resolved reflectivity for GaAs[14] and time-resolved x-ray diffraction for InSb[5], Si[15], Ge[10] and Bi[16]. Ultrafast melting takes place in the surface layer of the material on a timescale of a few hundred fs, although results vary with laser fluence. Within the domain of solid-solid nonthermal phase transitions, there has been a focus on VO_2, a monoclinic insulator that transforms into a metallic rutile phase under laser irradiation. Although the insulator-metal transition has been shown to occur within 200 fs, the time scale of the structural phase transition remains controversial. This is due to uncertainties in the rate of nucleation and growth, and to the disputed nature of the phase transition, which could take place anywhere between 100 fs and 100 ps[17–19].

Laser-induced phase transformations in covalent bonded materials and semiconductors are predominantly modeled using first principle methods and molecular-dynamics simulations[13,15,20–25]. Semiconductors such as Si show a large phonon softening and instability of the transverse acoustic mode in the whole Brillouin Zone (BZ) with increasing electronic temperature. In contrast, phonons of metals, such as Al and Au, are predicted to harden as the electronic temperature increases. However, the size of the effect strongly depends on the interplay between the lattice and the electronic structure. In Au, where the electronic DOS is dominated by the fully-filled d-band which its upper edge barely cross the Fermi energy, increases in electron temperature can lead to a change in the electronic DOS near the Fermi level. This results in a strong electron-phonon coupling, which in turn leads to a more pronounced phonon hardening[1]. Conversely, in Al, the electronic DOS remains nearly constant with temperature due to its free-electron-like behaviour, leading to weaker electron-phonon coupling and less pronounced phonon hardening. The potential hardening of phonon modes, which has also been suggested for other transition metals[1], stabilizes the metallic lattice and delays the solid-liquid phase transition[2]. In this work we argue that the metallic lattice stabilization also depends on the magnetic properties, and show that Fe, a partially filled d-band metal, can experience phonon softening, rather than hardening, due to demagnetization.

While the ultrafast demagnetization of ferromagnetic metals via electron excitations induced by femtosecond laser pulses has been studied for some time[26–32] our understanding of this process remains incomplete. This is mostly because the mechanisms behind laser-induced ultrafast demagnetization depend on the complex interaction of photons, electrons, spins, and the lattice, across a range of different timescales. The process can be simplified using a mean-field-like approach, within the following phenomenological three-temperature model. Initially, high-energy photons are absorbed, generating hot electrons that rapidly equilibrate to form an equilibrated electron liquid with a temperature of $T_{\rm el}$. Then, electron-phonon coupling acts to equilibrate these hot electrons with the lattice, thermalizing the system to a new temperature of $T_{\rm el-ph}$. Finally, the spin system which is characterized by an effective spin temperature of $T_{\rm spin}$, interacts with the electrons and phonons. We thus expect the timescale of magnetization change to be determined by the equilibration processes of electron-electron, electron-phonon, and electron-spin interactions. Never-

theless, even within this simplified model, quantifying all the relevant physical processes remains a formidable computational task.

In this study, we investigate the relationship between the topology of the Fermi surface, demagnetization, and a solid-solid nonthermal phase transition in Fe, using finite-temperature density functional theory (DFT)[33,34] and density functional perturbation theory (DFPT)[35]. The phase diagram, spin dynamics, correlation effects, and electronic structure properties of iron has widely been studied using numerous theoretical methods and experimental techniques[36–44]. At the ambient conditions, iron adopts the body-centred cubic (BCC) phase but transforms to a more thermodynamically stable face-centred cubic (FCC) phase called γ-Fe at a temperature of 1170 K. This $\alpha-\gamma$ phase transition has been extensively studied due to its practical applications and importance in material science[45]. At 1660 K, the FCC phase undergoes a reverse transformation to BCC, which eventually melts just above 1800 K[46]. It is known that the γ-Fe phase in the ground state has spin spiral non-collinear magnetic properties, with a spiral vector which strongly depends on the lattice parameter[47–49]. Here we do not consider non-collinear magnetism, and note that this assumption may have an impact on the detailed shape of the phase diagram for Fe. We aim to address features of this nature in future work.

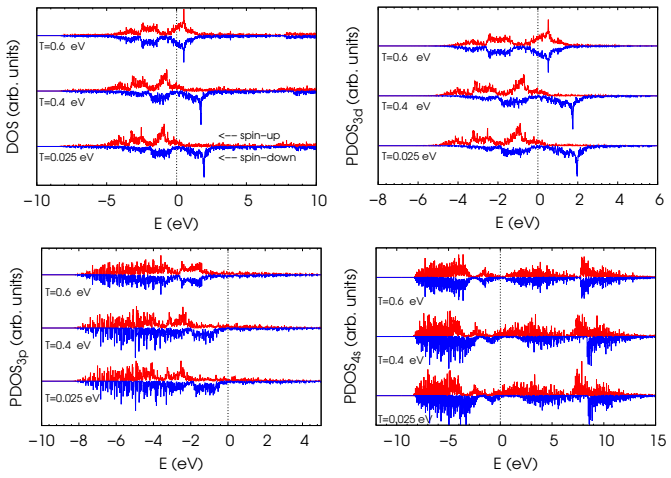

FIG. 1. Spin-polarised total electronic density of states (DOS) (top-left panel), 3d-orbital projected DOS (top-right panel), 3p-orbital projected DOS (bottom-left panel), and 4s-orbital projected DOS (bottom-right panel) of BCC-Fe at electronic temperatures of $T_{el} = 0.025, 0.4, 0.6$ eV. The dotted vertical line is the Fermi energy at room temperature. The maximum values of $\mathrm{PDOS_{3d}}$, $\mathrm{PDOS_{3p}}$, and $\mathrm{PDOS_{4s}}$ are 4.1, 0.0045, 0.44 (states /(eV Cell)), respectively. The density of states vicinity of the Fermi energy is dominated by 3d-band electrons at all temperatures. The demagnetization of BCC-Fe at $T \sim 0.6$ eV is evident.

II. COMPUTATIONAL DETAILS

To investigate the various Fe structures we use the Quantum Espresso package[50], with the Perdew-Burke-Ernzerhof (PBE) parameterization[51] of the exchange-correlation (XC) functional with a spin-polarized generalized-gradient correction. We will consider BCC and FCC crystal structures of Fe at electronic temperatures up to 3 eV, using a kinetic-energy cutoff of the plane-wave basis set of 120 Ry and an augmentation charge energy cutoff of 960 Ry. The finite-temperature DFT and DFPT calculations were carried out using a $(32, 32, 32)$ **k**-grid and a $(8, 8, 8)$ **q**-grid, respectively. The projector augmented wave (PAW) pseudopotential[52,53] was generated using the scalar-relativistic calculation with 16 valence electrons. The electronic temperature is controlled by the standard Fermi-Dirac distribution function. The number of empty bands is increased by the electronic temperature.

III. RESULTS AND DISCUSSIONS

A. Demagnetization of radiated Iron

We considered BCC and more close-packed FCC crystal structures of Fe over a range of electronic temperatures up to 3 eV. The spin-polarized electronic density of states (DOS) and the projected DOS (PDOS) of BCC-Fe obtained at three different electronic temperatures of $T_{el} = 0.025, 0.4, 0.6$ eV are shown in Fig. 1. At low temperatures we see the system is ferromagnetic: the majority of the spin-down channel sits above the Fermi energy, while the spin-up DOS sits below. The energy separation between spin-up and down electrons is mainly dominated by the d-band, with maximum values of the $3d$, $3p$, and $4s$ PDOS of 4.1, 0.0045, and 0.44 (states eV^{-1} cell^{-1}), respectively.

The projected density of states indicates that the DOS vicinity of the Fermi energy is dominated by the d-band. The magnetic interaction at low temperatures causes spin splitting of the d-bands in a way that the spin-up bands are almost filled, while in the spin-down bands, the Fermi energy is located in the area of relatively low DOS. In these situations, the gain in the exchange energy compensates for enlarging the electron kinetic energy and consequently forces the ferromagnetic state to be stable compared with the paramagnetic state. We do not take into account the on-site Hubbard U interaction in our analysis; we consider the Stoner nature of ferromagnetism in this study. As the temperature increases, the energy separation between spin-up and spin-down electrons decreases, eventually destroying the ferromagnetic ordering at an electronic temperature of $T_c \simeq 0.62$ eV. We note that this value will be subject to some uncertainty since our simplified calculations neglect the true elementary excitations in the form of spin waves and are impacted by the choice of XC functional and the inaccu-

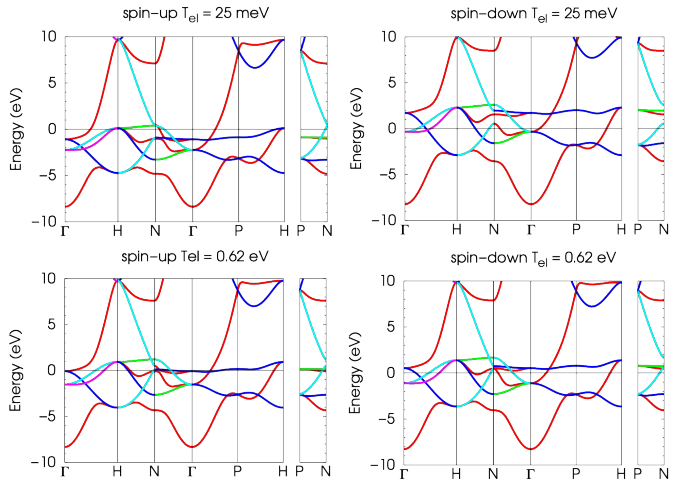

FIG. 2. Spin-dependent electronic band structure of BCC-Fe at electronic temperature T_{el} =0.025 and 0.62 eV. Up-shifting of spin-up and down-shifting of spin-down bands near the Fermi energy can be observed by increasing the electronic temperature. The bands are colored based on their point groups.

racy of DFT without Hubbard U parameter in describing the electronic and magnetic properties of strongly correlated transition metals.

Our calculations of the band structure of BCC-Fe are shown in Fig. 2, which indicate that the almost-filled spin-up d-band moves upward the Fermi energy, whereas the spin-down d-band downward the Fermi level by increasing the temperature until they almost overlap at T_{el}=0.62 eV enlarging DOS near the Fermi level. Hence, the energy ordering of spin-up and spin-down d-bands with respect to the Fermi energy behaves differently as a function of T_{el}, which ultimately results in a ferromagnetic to a paramagnetic phase transition. The average bandwidth of spin-up bands crossing the Fermi energy is much larger than that for spin-down bands. Because of the smaller dispersion of the down bands, increasing the temperature affects the spin-down bands more than the spin-up bands.

Our analysis also shows that the effect of electronic temperature on the ordering of spin-polarized d-bands significantly changes the Fermi surface topology and band degeneracies, which in turn affects the energy dispersion near band crossings and determines the nature of quasiparticles[54]. The Fermi surface (FS) of the two spin-down bands crossing the E_F is shown in Fig. 3 for electronic temperatures of 0.025 and 0.62 eV. The Fe-BCC bands are plotted inside the first Brillouin zone (BZ). By increasing the temperature, the bandwidths of the spin-down bands are reduced, resulting in further localization of the spin-down bands near E_F, and a modification of the topology of the FS near the BZ boundaries where the phonon dispersion anomaly occurs. The electronic excitations also modify the Fermi wave vector $\mathbf{k}_F$ and sharpen the Fermi surface, which can introduce a Kohn anomaly in the phonon spectra, which we discussed further in the following.

B. Phonon hardening and softening

To evaluate the dynamic stability of the two phases under electronic excitations, we calculate the phonon band structure as a function of electronic temperature. The FCC phase displays mechanical instability at low temperature (25 meV), which manifests through imaginary phonon frequencies along the $\Gamma - \mathrm{K}$ direction, as shown in Fig 5. In contrast, we see in Fig. 4 that BCC-Fe does not display imaginary phonons at the same temperature, indicating that Fe adopts the BCC structure at low temperatures. As the electronic temperature increases, the phonon dispersion curves of BCC-Fe show the appearance of soft modes along the $\Gamma - \mathrm{N}$ lines. A softening of a branch in the whole BZ disorders the lattice, whereas a phonon softening along high-symmetry points in the BZ could be a sign of a nonthermal solid-solid phase transition.

The phonon dispersion curves of BCC-Fe show the appearance of an anomalous dip in the lowest branch of the transverse-acoustic modes along the $\Gamma - \mathrm{N}$ direction at electronic temperatures between 0.62 and 1.0 eV. This anomaly results from a qualitative change in the electronic screening due to the modification of the electron-phonon coupling with electronic temperature. Importantly, we observe that BCC-Fe undergoes phonon softening before demagnetising and transitioning to the FCC phase. This is in contrast to the standard expectation for metals to exhibit phonon hardening under ultrafast laser radiation. For instance, Au was predicted to phonon harden with electron heating, leading to a sharp increase in its melting temperature[1,55]. For Fe, such behaviour can be seen in Fig. 5 for paramagnetic FCC-Fe, where we calculate a rise in the Debye temperature and, consequently, an increase in the melting temperature. Our results indicate that the vibrational response of metals to ultrafast laser pulses depends not only on the electronic structure but also on the magnetic properties of the system. Interestingly, the two processes compete, and the demagnetisation of a partially d-band-filled ferromagnetic metal leads to a softening of modes and a lowering of the melting temperature. We speculate the same scenario for other partially d-band-filled ferromagnetic transition metals.

Analysing the phonon spectra throughout the whole BZ of BCC-Fe at temperatures above 0.6 eV exhibits that the imaginary frequencies introducing dynamical instabilities take place in a localised region in $\mathbf{q}$-space. The localisation nature of the anomaly in the reciprocal space originates from the electronic structure. According to the definition of Kohn anomalies, a screening introduced by the electronic state close to the Fermi energy in metals, which is involved in the electron-phonon coupling, can generate anomaly dips in the phonon band structure.

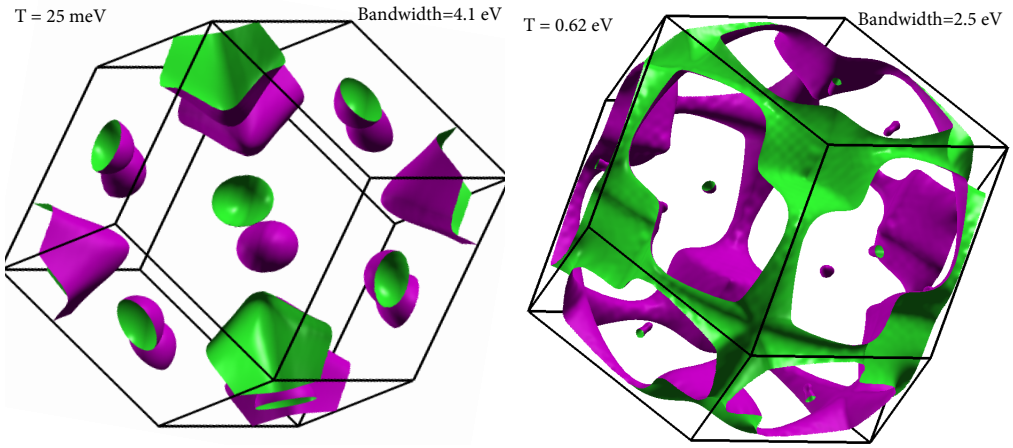

FIG. 3. Fermi surface of two spin-down bands at electronic temperature 0.025 and 0.62 eV plotted inside the first BZ of BCC structure. Increasing the electronic temperature reduces the bandwidth and localises the band near the Fermi surface.

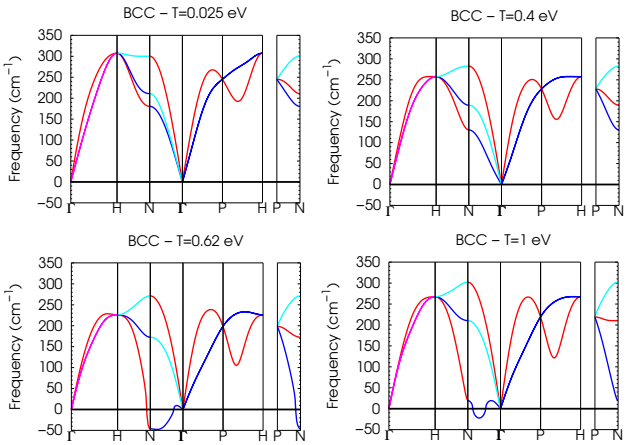

FIG. 4. Phonon dispersion curve of BCC-Fe at $T_{el} = 0.025, 0.4, 0.62, 1.0$ eV. Phonon softening can be observed by increasing the temperature from 0.025 to 0.4 eV. Further raising the temperature from 0.4 to 0.62 eV, where the demagnetization takes place, causes the appearance of imaginary phonons. At temperature 1 eV, in which the system has already been demagnetized, imaginary phonons start disappearing and the phonon dispersion curve exhibits phonon hardening. The bands are colored based on their point groups.

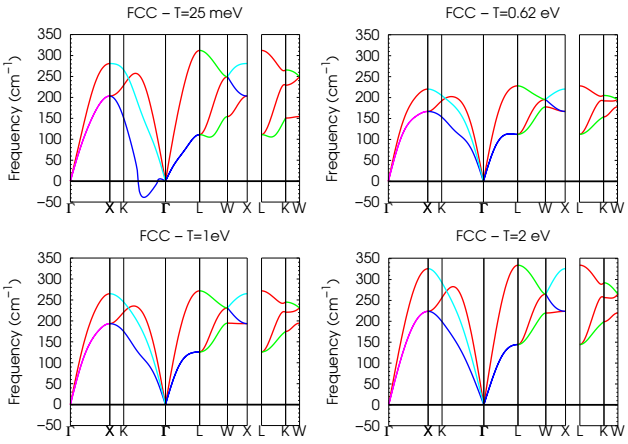

FIG. 5. Phonon dispersion curve of FCC-Fe at $T_{el} = 0.025, 0.62, 1.0, 2.0$ eV. Imaginary phonons at T = 0.025 eV indicate that the FCC is not a stable Fe crystal structure but BCC. At T=0.62 eV, where BCC-Fe becomes unstable, and the absolute magnetization vanishes Fig. 4, the FCC structure becomes stable with a large phonon softening. The phonon hardening can be observed by increasing the temperature to 1 and 2 eV. The bands are colored based on their point groups.

The existence of these anomalies is affected by the Fermi surface and the $\mathbf{q}$ functionality of the electron-phonon coupling matrix. If the temperature-modified FS adopts a flat area with nesting vector $\mathbf{q}_{\text{ano}}$, there could be a large screening of the potential perturbation because of atomic displacements at $\mathbf{q}_{\text{ano}}$, which leads to a softening that is localised in reciprocal space. The size of the Kohn anomaly is sensitive to the electronic temperature, and increasing the electronic temperature can reduce the sharpness of the FS and weaken the anomaly. This effect can be observed from the phonon dispersions of Fe-BCC at 0.62 and 1 eV in Fig. 4.

In contrast, we see in Fig. 5 that the phonon dispersion curves for paramagnetic FCC-Fe at temperatures above T_c do not show any anomalies or imaginary phonons but instead exhibit phonon hardening. We calculated the elastic constants tensor and obtained bulk, Young, and shear moduli and the Debye temperature θ_D of FCC-Fe at electronic temperatures of 0.62 and 3 eV. According to Debye-Lindemann's theory, the melting temperature T_m is related to θ_D as $T_m = C\,\theta_D^2$, where C depends on the atom's mass and density. Comparing the Debye temperature at 0.62 and 3 eV reveals an increase in the melting temperature by a factor of 1.25. For Au increasing the electronic temperature from 1 to 3 eV is predicted to increase the melting temperature by a factor of 1.44, which was attributed to the localization and large shift of

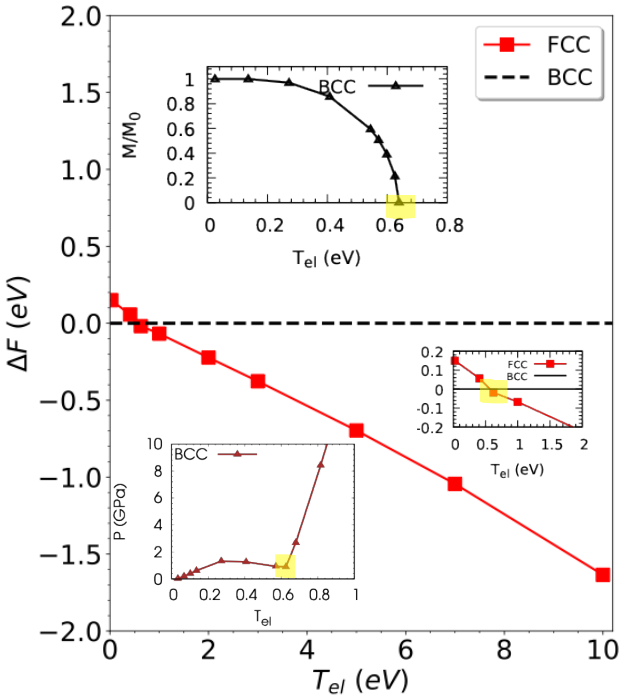

FIG. 6. The relative Helmholtz free energy ΔF as a function of electronic temperature T_{el}. The up inset shows the absolute magnetization (M) of BCC divided by its value at zero temperature (M_0) as a function of electronic temperature. The bottom-right inset shows the solid-solid BCC-FCC phase transition. The bottom-left inset shows the sudden jump in DFT predicted pressure P for BCC as a function of electronic temperature. The BCC demagnetization, BCC-FCC phase transition, and the sharp rise of P all occur at $T_{el} \sim 0.62$ eV highlighted by yellow colour.

the fully filled $5d$-bands to lower energies[1]. We observe a similar shift and localization in Fe with increasing electronic temperature, but these effects are less pronounced due to the partial filling of the $3d$ band.

C. Phase diagram

The absolute magnetization of BCC-Fe as a function of electronic temperature (Fig. 6) shows that demagnetization occurs at $T_{el} = 0.62$ eV, nearly six times higher than the Curie temperature of Fe. Figure 6 shows the Helmholtz free energy of the FCC phase with respect to the BCC phase, including both electronic and lattice contributions. Importantly, note that the non-thermal solid-solid phase transition takes place at the same temperature as the demagnetization, from which we conclude that the BCC-FCC transition coincides with the ferromagnetic-paramagnetic phase transition.

In contrast to semiconductors, where optical irradiation causes a phonon softening resulting in nonthermal melting[5], the melting process in metals is a thermal process requiring energy transfer from excited electrons to the ions[25,56]. Femtosecond electron diffraction measurements[2] provided support for phonon hardening in Au and showed increasing lattice stability at high electronic temperatures, confirmed by first principle simulations[1,55]. In contrast, ultrafast laser excitation measurements of Au observed the heterogeneous coexistence of solid and liquid and evidenced a heterogeneous to homogeneous melting transition[56], which can be related to atomic bond softening.

Our results predict that phonon hardening or softening in magnetic transition metals under optical irradiation could be related to the compressive Coulomb stress caused by electronic entropy, $-TS$ term in Helmholtz free energy. As illustrated in Fig. 6, the DFT predicted hot electron pressure P jumps at the demagnetization temperature, driving the structural transformation. The response of cold ions to this rapid change in photo-excited electron pressure could be either phonon softening if a structural transition occurs, such as a BCC to FCC phase transition, or phonon hardening if the crystalline unit cell volume is confined and no structure is energetically available for the transition. The BCC and FCC structures have packing factors of 0.68 and 0.74, respectively. So the ratio of their packing factors ~ 0.92 is close to one and both have $c/a = 1$, where c and a are the lattice parameters in z- and x-y-directions, respectively. Hence, a relatively small change of 1.1 GPa in the internal pressure can cause a structural transition. The effect of hot electron pressure can also be explained using the homogeneous electron gas (HEG) model[57] which is widely used in developing exchange-correlation DFT functionals[58]. At zero temperature, there is a difference between the pressure of spin-unpolarised and spin-polarized HEG at the same density. Hence, losing the spin-polarization due to electronic temperature introduces a gradient in electronic pressure. The response of cold ions to this gradient manifests itself either in the crystal transformation or in the phonon spectra.

IV. CONCLUSION

In summary, combining the Helmholtz free energy phase diagram, the absolute magnetization of BCC-Fe as a function of temperature, and the phonon dispersion curves, we find that BCC-Fe becomes dynamically unstable due to electronic excitations on ultrafast timescales. This instability leads to a decrease in its Debye temperature and in the absolute magnetisation until the system transforms to the paramagnetic-FCC phase. This phase, in contrast, experiences phonon hardening as the electron temperature is increased further. Our DFT simulations predict a non-thermal solid-solid phase transition takes place in Fe at an electron temperature of 0.62 eV, leading to an overall 25% increase in the melting temperature of Fe due to phonon hardening.

V. ACKNOWLEDGEMENT

The authors acknowledge support from the UK EPSRC grant EP/W010097/1 and from the Royal Society.

* sam.azadi@physics.ox.ac.uk

[1] V. Recoules, J. Clérouin, G. Zérah, P.M. Anglade, and S. Mazevet, "Effect of intense laser irradiation on the lattice stability of semiconductors and metals." Phys. Rev. Lett. **96**, 055503 (2006).

[2] R. Ernstorfer and et al., "The formation of warm dense matter: experimental evidence for electronic bond hardening in gold," Science **323**, 1033 (2009).

[3] K. Widmann, T. Ao, M. E. Foord, D. F. Price, A. D. Ellis, P. T. Springer, and A. Ng, "Single-state measurement of electrical conductivity of warm dense gold," Phys. Rev. Lett. **92**, 125002 (2004).

[4] A. M. Linderberg and et al., "Atomic-scale visualization of inertial dynamics," Science **308**, 392 (2005).

[5] A. Rousse, C. Rischel, S. Fourmaux, I. Uschmann, S. Sebban, G. Grillon, Ph. Balcou, E. Foerster, J.P. Geindre, P. Audebert, J.C. Gauthier, and D. Hulin, "Non-thermal melting in semiconductors measured at femtosecond resolution," Nature (London) **410**, 65 (2001).

[6] N. Medvedev and I. Milov, "Nonthermal phase transitions in metals," Scientific Reports **10**, 12775 (2020).

[7] G. Sciaini and R. J. D. Miller, "Femtosecond electron diffraction: heralding the era of atomically resolved dynamics," Rep. Prog. Phys. **74**, 096101 (2011).

[8] E. Collet and et all., "Laser-induced ferroelectric structural order in an organic charge-transfer crystal," Science **300**, 612 (2003).

[9] J.G. Fujimoto, J.M. Liu, and E.P. Ippen, "Femtosecond laser interaction with metallic tungsten and nonequilibrium electron and lattice temperatures," Phys. Rev. Lett. **53**, 1837 (1984).

[10] C.W. Siders, "Detection of nonthermal melting by ultrafast x-ray diffraction," Science **286**, 1340 (1999).

[11] S.K. Sundaram and E. Mazur, "Inducing and probing nonthermal transitions in semiconductors using femtosecond laser pulses," Nat. Mat. **1**, 217 (2002).

[12] N. Medvedev, "Nonthermal phase transitions in irradiated oxides," J. Phys.: Condens. Matter **32**, 435401 (2020).

[13] K. Sokolowski-Tinten, C. Blome, C. Dietrich, A. Tarasevitch, M. Horn von Hoegen, and D. von der Linde, "Femtosecond x-ray measurement of ultrafast melting and large acoustic transients," Phys. Rev. Lett. **87**, 225701 (2001).

[14] P. Saeta, J.-K. Wang, Y. Siegal, N. Bloembergen, and E. Mazur, "Ultrafast electronic disordering during femtosecond laser melting of gaas," Phys. Rev. Lett. **67**, 1023 (1991).

[15] M. Harb, R. Ernstorfer, C. T. Hebeisen, G. Sciaini, W. Peng, T. Dartigalongue, M. A. Eriksson, M. G. Lagally, S. G. Kruglik, and R. J. D. Miller, "Electronically driven structure changes of Si captured by femtosecond electron diffraction," Phys. Rev. Lett. **100**, 155504 (2008).

[16] K. Sokolowski-Tinten, C. Blome, J. Blums, A. Cavalleri, C. Dietrich, A. Tarasevitch, I. Uschmann, E. Förster, M. Kammler, M. Horn von Hoegen, and D. von der Linde, "Femtosecond x-ray measurement of coherent lattice vibrations near the lindemann stability limit," Nature **422**, 287 (2003).

[17] A. Cavalleri, Cs. Tóth, C.W. Siders, J. A. Squier, F. Ráksi, P. Forget, and J. C. Kieffer, "Femtosecond structural dynamics in VO_2 during an ultrafast solid-solid phase transition," Phys. Rev. Lett. **87**, 237401 (2001).

[18] S. Wall, S. Yang, L. Vidas, M. Chollet, M. Glownia, M. Kozina, T. Katayama, T. Henighan, M. Jiang, T. A. Miller, D. A. Reis, L. A. Boatner, O. Delaire, and M. Trigo, "Ultrafast disordering of vanadium dimers in photoexcited VO_2," Science **362**, 572 (2018).

[19] A. S. Johnson, D. Perez-Salinas, K. M. Siddiqui, Sungwook Choi S. Kim3, K. Volckaert, P. E. Majchrzak, S. Ulstrup, N. Agarwal, K. Hallman, R. F. Haglund Jr, C. M. Guünther, B. Pfau, S. Eisebitt, D. Backes, F. Maccherozzi, A. Fitzpatrick, S. S. Dhesi, P. Gargiani, M. Valvidares, N. Artrith, F. de Groot, H. Choi, D. Jang, A. Katoch, S. Kwon, S. Han Park, H. Kim, and S. E. Wall, "Ultrafast x-ray imaging of the light-induced phase transition in VO_2," Nat. Phys. **19**, 215 (2022).

[20] P. Stampfli and K. H. Bennemann, "Theory for the instability of the diamond structure of Si, Ge, and C induced by a dense electron-hole plasma," Phys. Rev. B **42**, 7163 (1990).

[21] P. Lorazo, L. J. Lewis, and M. Meunier, "Short-pulse laser ablation of solids: From phase explosion to fragmentation," Phys. Rev. Lett. **91**, 225502 (2003).

[22] S. Williamson, G. Mourou, and J. C. M. Li, "Time-resolved laser-induced phase transformation in aluminum," Phys. Rev. Lett. **52**, 2364 (1984).

[23] P. L. Silvestrelli, A. Alavi, M. Parrinello, and D. Frenkel, "Ab initio molecular dynamics simulation of laser melting of silicon," Phys. Rev. Lett. **77**, 3149 (1996).

[24] Tobias Zier, Eeuwe S. Zijlstra, and Martin E. Garcia, "Quasimomentum-space image for ultrafast melting of silicon," Phys. Rev. Lett. **116**, 153901 (2016).

[25] B. J. Siwick, J. R. Dwyer, R. E. Jordan, and R. J. D. Miller, "An atomic-level view of melting using femtosecond electron diffraction," Science **302**, 1382 (2003).

[26] E. Beaurepaire, J.-C. Merle, A. Daunois, and J.-Y. Bigot, "Ultrafast spin dynamics in ferromagnetic nickel," Phys. Rev. Lett **76**, 4250 (1996).

[27] J. Hohlfeld, E. Matthias, R. Knorren, and K. H. Bennemann, "Nonequilibrium magnetization dynamics of nickel," Phys. Rev. Lett. **78**, 4861 (1997).

[28] G. P. Zhang and W. Hübner, "Laser-induced ultrafast demagnetization in ferromagnetic metals," Phys. Rev. Lett. **85**, 3025 (2000).

[29] B. Koopmans, J. J. M. Ruigrok, F. Dalla Longa, and W. J. M. de Jonge, "Unifying ultrafast magnetization dynamics," Phys. Rev. Lett. **95**, 267207 (2005).

[30] K. Carva, M. Battiato, and P. M. Oppeneer, "Ab initio investigation of the elliott-yafet electron-phonon mechanism in laser-induced ultrafast demagnetization," Phys. Rev. Lett. **207201**, 207201 (2011).

[31] Andrei Kirilyuk, Alexey V. Kimel, and Theo Rasing, "Ultrafast optical manipulation of magnetic order," Rev. Mod. Phys. **82**, 2731 (2010).

[32] A. L. Chekhov, Y. Behovits, J. J. F. Heitz, C. Denker, D. A. Reiss, M. Wolf, M. Weinelt, P.W. Brouwer, M. Muünzenberg, and T. Kampfrath, "Ultrafast demagnetization of iron induced by optical versus terahertz pulses," Phys. Rev. X **11**, 041055 (2021).

[33] N. D. Mermin, "Thermal properties of the inhomogenous electron gas," Phys. Rev. **137:A**, 1441 (1965).

[34] A. Pribram-Jones, S. Pittalis, E.K.U. Gross, and K. Burke, "Thermal density functional theory in context," Frontiers and Challenges in Warm Dense Matter **25**, 60 (2014).

[35] Stefano Baroni, Stefano de Gironcoli, Andrea Dal Corso, , and Paolo Giannozzi, "Phonons and related crystal properties from density-functional perturbation theory," Rev. Mod. Phys. **515**, 2001 (73).

[36] J. Sánchez-Barriga, J. Fink, V. Boni, I. Di Marco, J. Braun, J. Minar, A. Varykhalov, O. Rader, V. Bellini, F. Manghi, H. Ebert, M. I. Katsnelson, A. I. Lichtenstein, O. Eriksson, W. Eberhardt, and H. A. Dürr, "Strength of correlation effects in the electronic structure of iron," Phys. Rev. Lett. **103**, 103, 267203 (2009).

[37] R. Lizárraga, L. Nordström, O. Eriksson, and J. Wills, "Noncollinear magnetism in the high-pressure hcp phase of iron," Phys. Rev. B **78**, 064410 (2008).

[38] H. Ma, S. L. Qiu, and P. M. Marcus, "Pressure instability of bcc iron," Phys. Rev. B **66**, 024113 (2002).

[39] P. M. Marcus, V. L. Moruzzi, and S.-L. Qiu, "Tetragonal equilibrium states of iron," Phys. Rev. B **60**, 369 (1999).

[40] V. L. Moruzzi, P. M. Marcus, and P. C. Pattnaik, "Magnetic transitions in bcc vanadium, chromium, manganese, and iron," Phys. Rev. B **37**, 8003 (1988).

[41] H. Ma, S. L. Qiu, and P. M. Marcus, "Pressure instability of bcc iron," Phys. Rev. B **66**, 024113 (2002).

[42] P. M. Marcus and V. L. Moruzzi, "Stoner model of ferromagnetism and total-energy band theory," Phys. Rev. B **38**, 6949 (1988).

[43] S. L. Qiu, P. M. Marcus, and Hong Ma, "Epitaxial bain path of tetragonal Fe," Phys. Rev. B **61**, 104431 (2001).

[44] V. L. Moruzzi, P. M. Marcus, K. Schwarz, and P. Mohn, "Ferromagnetic phases of bcc and fcc Fe, Co, and Ni," Phys. Rev. B **34**, 1784 (1986).

[45] I. Leonov, A. I. Poteryaev, V. I. Anisimov, and D. Vollhardt, "Calculated phonon spectra of paramagnetic iron at the α-γ phase transition," Phys. Rev. B **85**, 020401(R) (2012).

[46] D. A. Porter and K. E. Easterling, *Phase Transformations in Metals and Alloys, 2nd ed.* (Chapman and Hall, London, 1992).

[47] K. Knöpfle, L.M. Sandratskii, and J. Kübler, "Spin spiral ground state of γ-iron," Phys. Rev. B **62**, 5564 (2000).

[48] L. Kleinman, "Density functional for noncollinear magnetic systems," Phys. Rev. B **59**, 3314 (1998).

[49] D. M. Bylander and L. Kleinman, "Full-potential generalized gradient approximation calculations of spiral spin-density waves in γ-Fe," Phys. Rev. B **59**, 6278 (1998).

[50] P. Giannozzi and et al., "Quantum espresso: a modular and open-source software project for quantum simulations of materials," Journal of physics: Condensed matter **39**, 395502 (2009).

[51] John P. Perdew, Kieron Burke, and Matthias Ernzerhof, "Generalized gradient approximation made simple," Phys. Rev. Lett. **77**, 3865 (1996).

[52] P. Giannozzi et al., "Advanced capabilities for materials modelling with quantum espresso," J. Phys.: Condens. Matter **29**, 465901 (2017).

[53] G. Kresse and D. Joubert, "From ultrasoft pseudopotentials to the projector augmented-wave method," Phys. Rev. B **59**, 1758 (1999).

[54] S. Azadi, N.D. Drummond, and W.M.C. Foulkes, "Quasiparticle effective mass of the three-dimensional fermi liquid by quantum monte carlo," Phys. Rev. Lett. **127**, 086401 (2021).

[55] S. Mazevet, J. Clérouin, V. Recoules, P. M. Anglade, and G. Zerah, "Ab-initio simulations of the optical properties of warm dense gold," Phys. Rev. Lett. **95**, 085002 (2005).

[56] M. Z. Mo, Z. Chen, R.K.Li, M. Dunning, B.B.L.Witte, J. K. Baldwin, L. B. Fletcher, J. B. Kim, A.Ng, R. Redmer, A. H. Reid, P. Shekhar, X. Z. Shen, M. Shen, K. Sokolowski-Tinten, Y. Y. Tsui, Y. Q. Wang, Q. Zheng, X. J. Wang, and S. H. Glenzer, "Heterogeneous to homogeneous melting transition visualized with ultrafast electron diffraction," Science **360**, 6396 (2018).

[57] S. Azadi and N.D. Drummond, "Low-density phase diagram of the three-dimensional electron gas," Phys. Rev. B **105**, 245135 (2022).

[58] S. Azadi, N.D. Drummond, and S.M. Vinko, "Correlation energy of the paramagnetic electron gas at the thermodynamic limit," Phys. Rev. B **107**, L121105 (2023).